Geophys. J. Int. (2006) **165,** 865–874 doi: 10.1111/j.1365-246X.2006.02929.x

Attenuation anisotropy and the relative frequency content of split shear waves

Andrew J. Carter and J.-Michael Kendall*

Institute of Geophysics and Tectonics, School of Earth and Environment: Earth Sciences, University of Leeds, Leeds, LS2 9JT, *UK*

Accepted 2006 January 20. Received 2006 January 18; in original form 2004 October 14

SUMMARY

The variation of frequency-dependent seismic wave attenuation with direction (attenuation anisotropy) contains additional information to that contained in velocity anisotropy. In particular, it has the potential to distinguish between different mechanisms that can cause velocity anisotropy. For example, aligned fracturing might be expected to cause measurable velocity and attenuation anisotropy, while preferred crystal orientation leads to significant velocity anisotropy but may cause only small amounts of attenuation. Attenuation anisotropy may also contain useful information about pore-fluid content and properties. We present a methodology for analysis of attenuation anisotropy, and apply it to a microseismic data set previously analysed for shear-wave splitting by Teanby *et al.* (2004). Attenuation anisotropy values obtained show a temporal variation which appears to correlate with the temporal variation in the velocity anisotropy. The comparison of the relative frequency content of fast (S1) and slow (S2) split shear waves is a convenient method for examining seismic attenuation anisotropy. Provided that S1 and S2 initially have the same spectral colouring, that no spectral distortion is introduced by the differences between receiver responses of geophone components, and that spectral distortion due to background noise can be ignored or corrected for, we can attribute any differences in their frequency content to attenuation anisotropy. Attenuation anisotropy, where present, should be detected by the different (approximately orthogonal) polarizations of S1 and S2 as they pass through the anisotropic medium. In the presence of attenuation anisotropy S1 and S2 should experience different levels of frequency-dependent attenuation. We quantify the differential attenuation of S1 and S2 using a scheme based on a spectral ratio method. We present results from a microseismic data set acquired in an abandoned oil well at Valhall, a North Sea oil field. The results are surprising in that sometimes the slower arrival, S2, is richer in high frequencies than the faster, S1. This appears to be contrary to results predicted by theoretical crack models for attenuation anisotropy (e.g. Hudson 1981). The mechanism responsible for these observations is not clear. Our differential attenuation attribute correlates with the angle between the strike of the inferred initial shear-wave source polarization and the fast shear-wave polarization, which suggests that the split shear wave with the larger amplitude is preferentially attenuated. Our attribute also correlates with the event backazimuth, and the minimum percentage anisotropy.

Key words: attenuation, cracked media, microseismicity, seismic anisotropy, shear-wave splitting, spectral analysis.

1 INTRODUCTION

1.1 Fracture detection, anisotropy and shear-wave splitting

Fracture detection in rocks in the top few kilometres of the Earth's crust has several important applications. First, in geothermal applications water is pumped from an injector well through a fractured reservoir to a recovery well. The heating of the water during the flow

*Now at: Department of Earth Sciences, University of Bristol, Wills Memorial Building, Queen's Road, Bristol, BS8 1RJ, UK. E-mail: gljmk@bristol.ac.uk

can be used to generate electricity. Fracture detection and mapping is important in understanding the flow, since the route taken by the flow is controlled by the fracturing. Second, underground storage of carbon dioxide and radioactive waste both require unfractured sealing structures to avoid leakage. Fracture detection is, therefore, required in evaluating the suitability of structures for carbon dioxide and radioactive waste storage. Finally, efficient production of a hydrocarbon reservoir requires knowledge of fluid flow pathways and compartmentalization within the reservoir. Fracture size, fracture orientation and the amount of fracturing are all important parameters. The amount of fracturing, or fracture density, is a control on fracture-related permeability. Roughly speaking, the more fracturing, the better the permeability. Fracture orientation information allows the targeting of horizontal wells perpendicular to fracture strike to maximize the number of fractures cut by the wellbore, and hence increase production flow rates. Fracture size information is also useful since fractures of the order of metres in size are thought to be the most important for controlling permeability in hydrocarbon reservoirs (Maultzsch *et al.* 2003).

Fractures cause seismic velocities to depend on the direction of wave propagation, an effect called velocity anisotropy. For example, seismic *P* waves travelling perpendicular to fractures travel more slowly than *P* waves travelling parallel to the fractures. The expected velocity variation in directions between these two extremes depends on variables including rock matrix elastic constants, pore-fluid properties and saturations, the amount of fracturing and the arrangement and shape of the fractures.

Various schemes for modelling anisotropic wave propagation in fractured rocks exist. These schemes use different idealized models to represent the arrangement and shape of fractures. Some include fluid flow associated with only one length scale (e.g. Chapman *et al.* 2002; Crampin & Zatsepin 1997; Hudson 1981), others include fluid flow on more than one length scale (e.g. Chapman 2003), or restrict fluid flow to flow between particular parts of the pore space (e.g. Pointer *et al.* 2000). The modelling schemes also make different mathematical approximations in arriving at their predicted anisotropies, and not all make predictions regarding attenuation anisotropy. The effects of changes in ambient applied differential stress and pore-fluid pressure are also often ignored. Anisotropic poroelasticity (Crampin & Zatsepin 1997; Zatsepin & Crampin 1997) includes these effects but makes no predictions regarding the frequency-dependence of the predicted anisotropy. All of the anisotropic models mentioned require further validation against field data before we can be confident in the reliability and scope of their predictions. Measurement of attenuation anisotropy as well as velocity anisotropy from field data should help us decide which models best predict observed wave characteristics.

Velocity anisotropy measurements alone are insufficient to determine the mechanism causing the anisotropy. For example, crystal lattice preferred orientation and aligned fractures could in theory produce the same observed velocity anisotropy. However, the attenuation anisotropy produced by these two mechanisms should differ. Aligned fracturing might be expected to produce attenuation anisotropy at the frequencies used in field seismic experiments, while crystal lattice preferred orientation would not. Therefore, attenuation anisotropy measurements may allow us to distinguish between possible causes of observed velocity anisotropy.

Fractures cause seismic shear waves to split into two separate arrivals, referred to here loosely as split shear waves. These split shear waves are polarized approximately perpendicular to one another. For vertically propagating shear waves and vertical fractures, the faster split shear wave (S1) is polarized parallel to the fracture strike, the slower split shear wave (S2) is polarized perpendicular to the fracture strike. The difference in the arrival times of S1 and S2 is known as the splitting time.

Shear-wave splitting in the crust has been widely observed and studied, see Crampin & Chastin (2003) for a review. Shear-wave splitting contains information about fracture density and orientation. The fracture density information is contained in the splitting time. The strike of the fractures can be estimated from the polarization of S1. Temporal variations in shear-wave splitting parameters can also tell us about time-dependent changes in the stress field (Caley *et al.* 2001; Teanby *et al.* 2004). A growing number of workers have observed frequency-dependent shear-wave splitting (e.g. Chesnokov *et al.* 2001; Liu *et al.* 2002; Marson-Pidgeon & Savage 1997). However, such observations can be difficult to obtain given the limited signal bandwidth often available.

Two main types of mechanism are thought to cause frequency-dependent anisotropy. First, layering or heterogeneity on a length scale shorter than the seismic wavelength (e.g. Werner & Shapiro 1999) causes higher frequencies to have shorter splitting times than low frequencies. This happens because the higher frequencies are scattered by the layering or heterogeneity, while the lower frequencies experience an effective medium that appears to be anisotropic even if the thin layers are themselves isotropic (Backus 1962). Second, the flow of pore fluids from more compliant to less compliant parts of the pore space (including fractures) during the passage of a seismic wave can cause frequency-dependent shear wave splitting (e.g. Chapman 2003; Pointer *et al.* 2000; Thomsen 1995; Tod & Liu 2002). The frequency dependence of the splitting time may contain information about the predominant fracture size (Maultzsch *et al.* 2003; Chapman 2003). The presence of frequency-dependent shear-wave splitting requires frequency-dependent velocities (dispersion). Dispersion and intrinsic attenuation are necessarily linked (e.g. Aki & Richards 1980). Therefore, if dispersion is anisotropic, attenuation must also be anisotropic. Thus frequency-dependent shear-wave splitting and seismic attenuation anisotropy are necessarily linked.

Hudson (1981) produced a model predicting the velocity and attenuation anisotropy due to a dilute distribution of vertically oriented penny-shaped cracks. This model is strictly only valid in the high-frequency limit, for wavelengths that are long compared to the fracture scale. However, we have used this theory as an example, because it is an established theory which has been validated for some experimental conditions (Peacock *et al.* 1994; Rathore *et al.* 1995). Hudson (1981) predicts that the slower split shear wave (S2) should have its high frequencies preferentially attenuated relative to the faster split shear wave (S1) (see Appendix A). We find this prediction intuitively attractive since S1 should be less affected by the fractures both in terms of scattering by the fractures and in terms of fluid flow within and between the fractures and aligned porosity.

In this paper we present observations, made from a microseismic data set, of the relative frequency content of pairs of split shear waves. These observations allow testing of the Hudson (1981) predictions for the attenuation of split shear waves and could also be used to test the predictions of other theoretical models. Once a model is found which fits the observations, the difference in attenuation between pairs of split shear waves provides an additional observation with which to constrain inversions for rock and pore-fluid properties. Temporal variations in the attenuation anisotropy may also provide complementary information to that provided by temporal variation in splitting parameters. We present a methodology that is simple, and requires no extra acquisition costs beyond those required for the shear-wave splitting study. We assess the robustness of our

observations and compare our results with the predictions of the model of Hudson (1981). We find that approximately half of our observations show S2 to be richer in high frequencies than S1, apparently contradicting the predictions of the model.

1.2 Microseismic monitoring and shear-wave splitting analysis at the Valhall Field, North Sea

The aims, experimental design and results of the Valhall microseismic experiment are reported by Dyer *et al.* (1999). Shear-wave splitting analysis of the Valhall microseismic data is described in detail by Teanby *et al.* (2004). Only a few relevant points concerning the microseismic experiment will be covered here.

The Valhall field, in the Norwegian sector of the North Sea, is a field producing oil from the undersaturated and overpressured rocks of Upper Cretaceous chalks in the Tor and Hod formations. Production at Valhall causes subsidence in the overburden which is observable at the seafloor. This is the most probable cause of microseismic events which can be used to map active faults and to monitor stress in the reservoir (Teanby *et al.* 2004). In 1997, a vertical string of six three-component geophones was placed in an abandoned well above the reservoir near the crest of the field structure.

Over a period of 56 days microseismic events were continuously recorded yielding a data set of 572 events, 324 of which could be located reliably (Dyer *et al.* 1999). The majority of the events were located, above the reservoir, in the siltstone caprock at about 2 km depth, 300–500 m from the receivers. Source locations mostly group into two main clusters (Teanby *et al.* 2004). For the attenuation analysis that follows, results are considered from just from one cluster, the nearest cluster to the receivers, to eliminate path-dependent effects. The receiver geometry and event locations are shown in Fig. 1. Shear-wave splitting analysis revealed significant temporal variation in the amount of velocity anisotropy observed (Teanby *et al.* 2004). One of our aims was to see if a temporal variation in attenuation anisotropy is also present in these data.

2 METHODS

2.1 Methodology for differential attenuation analysis

The aim of this method is to obtain a useful measure of the difference in intrinsic attenuation experienced by a pair of split shear waves as they pass through a fractured medium. The differential attenuation attribute measured should be an estimate of a material property, rather than a measure that depends on the traveltime or distance spent in the attenuative medium. In forming the differential attenuation, intrinsic attenuation is assumed to be of a constant-Q type (Futterman 1962).

The inputs to our method (see Figs 2a–b for examples) are estimates of the fast (S1) and slow (S2) split shear waves output from a shear-wave splitting analysis (e.g. Teanby *et al.* 2004). We then calculate the differential attenuation, ΔQ^{-1}_{f-s}. Differential attenuation quantifies the difference in energy loss per cycle experienced by S1 and S2, averaged over the fractured part of the ray path. It is not a true quality factor measurement; it approximates the Q^{-1}, sometimes called specific attenuation, that a homogeneous constant-Q material would require to produce the observed difference in frequency content between S1 and S2. Differences between Q^{-1}_{S1} and Q^{-1}_{S2} are assumed to be evenly distributed between source and receiver so that the attribute is a minimum estimate, since parts of the ray path may exhibit neither velocity nor attenuation anisotropy.

Assuming that S1 and S2 are each made up of components with frequency f whose amplitudes obey,

$$A_{Sn}(f) = G_{Sn}(f)S_{Sn}(f)R_{Sn}(f)\exp\left(\frac{-\pi t_{Sn} f}{Q_{Sn}}\right), \quad (1)$$

where $A(f)$ is the recorded amplitude at the receiver, $G(f)$ is the transfer function of the geometric spreading, $S(f)$ is the amplitude at the source, $R(f)$ is the effective transfer function of the receivers (i.e. taking into account the rotation, the coupling, the impulse response of the geophone, and the recording system response), t is the source-to-receiver traveltime. The subscript n is 1 for the faster split shear wave and 2 for the slower split shear wave.

Assuming that S1 and S2 experienced the same geometrical spreading, the same effective receiver transfer function, and that S1 and S2 had the same spectral colouring at source, we can then use the spectral ratio method (Båth 1974) to measure the relative attenuation between the two waveforms. Other techniques for attenuation measurement could be used instead of spectral ratios if desired. We have used the spectral ratio method for simplicity.

We form the $\log_e$(amplitude spectral ratio) (LASR),

$$\ln\left(\frac{A_{S1}(f)}{A_{S2}(f)}\right) = -\pi\left(\frac{t_{S1}}{Q_{S1}} - \frac{t_{S2}}{Q_{S2}}\right) f + c. \quad (2)$$

The c term in the above equation arises from any frequency-independent differences in the G_{Sn}, S_{Sn} and R_{Sn} terms in eq. (1).

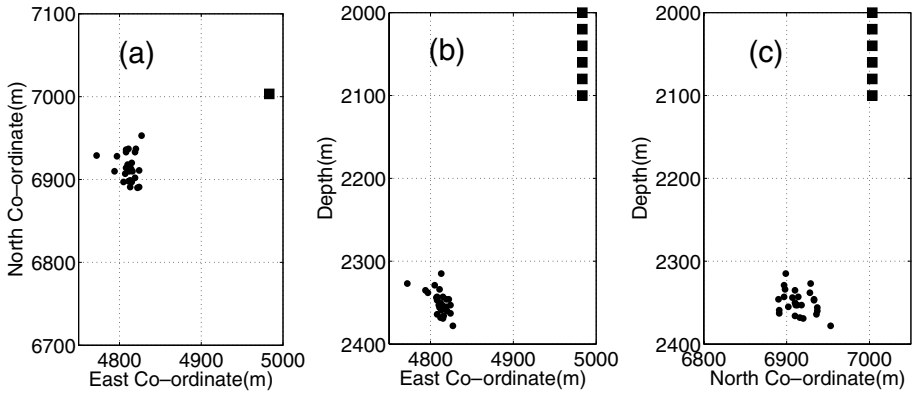

Figure 1. Locations of microseismic events which gave both reliable shear-wave splitting and differential attenuation measurements. Black circles show event locations and black squares show downhole geophone locations. The map view (a) and the depth sections (b) and (c) are all plotted at the same scale to allow visual assessment of angles of incidence and backazimuth.

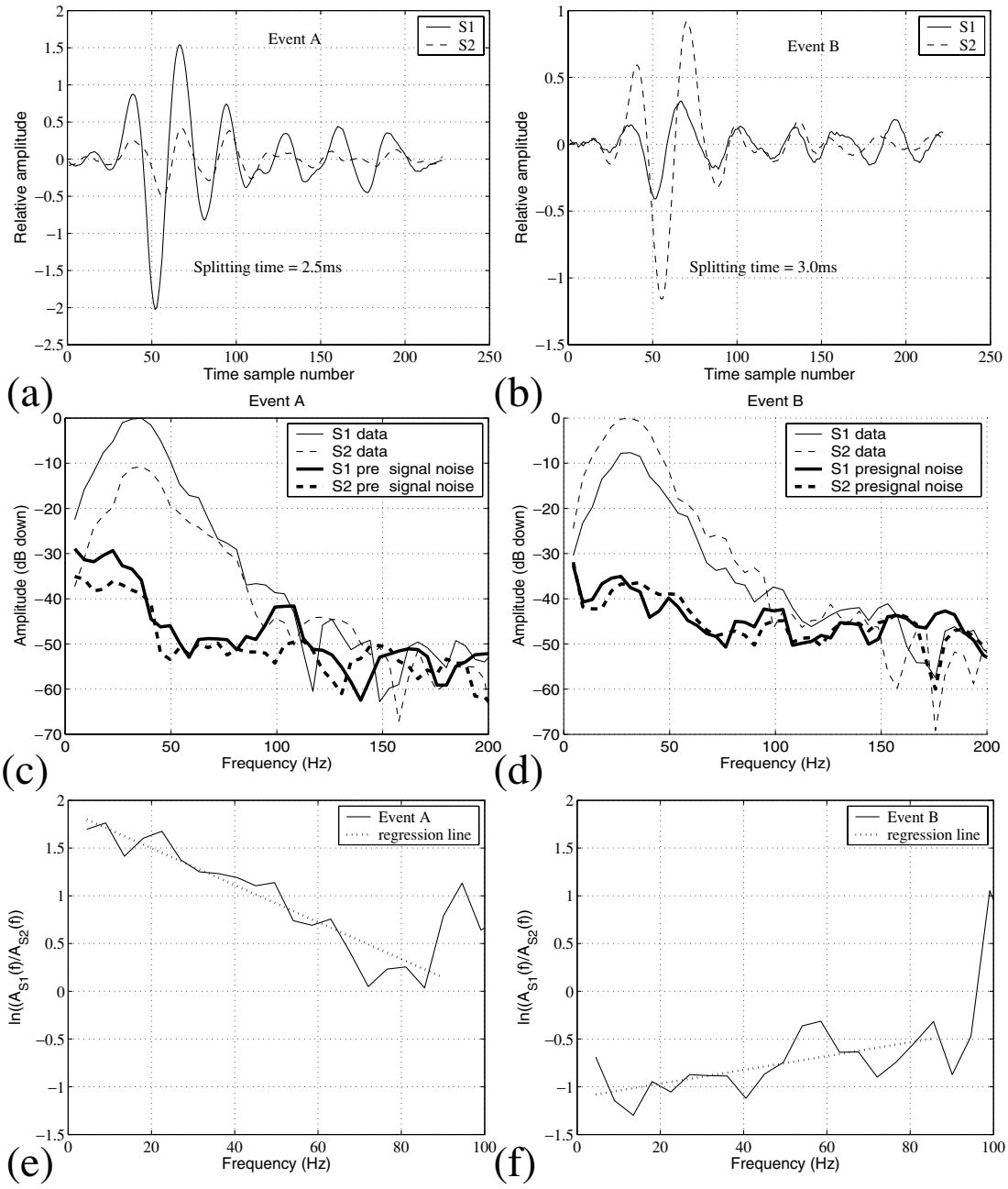

Figure 2. (a) Event A—an example of a splitting result exhibiting negative differential attenuation; (b) Event B—an example of a splitting result exhibiting positive differential attenuation; (c) Amplitude spectra of (a); (d) Amplitude spectra of (b); (e) Log_e (spectral ratio) formed from (c) and (f) Log_e (spectral ratio) formed from (d). Regression lines are shown in (e) and (f). The bandwidths over which the regressions were performed are indicated by the lateral extent of the dotted regression lines. Note that the frequency axes in (e) and (f) differ from those in (c) and (d).

For constant-Q attenuation the LASR should be approximately linear against frequency over the signal bandwidth (see Figs 2e–f for examples). We obtain the gradient using a least-squares linear regression of the LASR performed over a limited range of frequencies (regression bandwidth). The gradient is then divided by πt_{S1} to yield the attribute ΔQ^{-1}_{f-s},

$$\Delta Q^{-1}_{f-s} = \frac{t_{S2}}{t_{S1} Q_{S2}} - \frac{1}{Q_{S1}}. \tag{3}$$

In performing the spectral ratio analysis the regression must be performed over a suitable bandwidth and the data should be windowed and tapered appropriately (Spencer 1985; Pujol & Smithson 1991). The choice of regression bandwidth was made by comparison of the amplitude spectra for S1 and S2 with the spectra of their pre-event noise (e.g. see Figs 2c–d). The robustness of the results should be checked by variation of the window length and type (e.g. see Fig. 3), and if possible the regression bandwidth. The uncertainties output from the method were calculated using the uncertainties on the gradient estimated by the least-squares regression.

When the differential attenuation, ΔQ^{-1}_{f-s}, is negative, S1 is more attenuated than S2 (i.e. $Q^{-1}_{S1} > Q^{-1}_{S2}$). This arises from eq. (3) since the ratio t_{S2}/t_{S1} is always greater than one. However, when the

attribute is positive, strictly we cannot say which of the split shear waves has been more attenuated per cycle. This difficulty arises as without an estimate of either Q_{S1}^{-1} or Q_{S2}^{-1} we cannot say whether any additional loss of high frequencies experienced by S2 has come about purely because of the additional time (the splitting time) spent in the attenuative medium, or whether the losses are sufficient that we can say that S2 has genuinely experienced a greater attenuation per cycle (i.e. a higher Q^{-1}). For our data set however, Q_{S1}^{-1} would need to be greater than about $1/7$, that is, the rock would have to be extremely attenuative, in order to have both a positive ΔQ_{f-s}^{-1} and a preferentially attenuated fast split shear wave. For our data a positive value of differential attenuation, therefore, means that the slower split shear wave has, as we might intuitively expect, been preferentially attenuated compared to the faster split shear wave during propagation. Negative values of differential attenuation mean that the converse is true.

To ensure that our results are quantifying attenuation anisotropy and not other effects we must ensure that:

(i) The differential attenuation measurements are robust to small changes in the parametrization of the method, for example, the exact window length used in the analysis;

(ii) There are no differences between the receiver responses (including coupling) of individual components, which would appear in eq. (2);

(iii) That the effects of background noise on the spectra can be ignored or corrected for.

The first requirement was tested (see Section 3.2) by using a variety of window types and lengths in the analysis. The final window type and length used for the results presented here was a 222 ms long 2π adaptive multitaper. To test the robustness of the results we also checked that the differences in the dominant frequency of S1 and S2, derived both in the time and frequency domains, were consistent with the differential attenuation values (see Section 3.5). For example, if the differential attenuation is positive, the dominant frequency of S2 should be lower than that of S1.

The second requirement was tested by the examination of 'ping test' responses (see Section 3.4) used to check the impulse responses of individual geophone components. The third requirement relates to the biasing effect of additive noise on the signal spectral estimates. This biasing effect does not cancel when $\log_e$ (spectral ratios) are formed, and is one of the main weaknesses of spectral ratio methods for attenuation analysis. We have addressed this issue by also using frequency-domain matching filters (Raikes & White 1984) instead of spectral ratios, but found that this method made no improvement, perhaps because after rotation the noise on the input traces was correlated. We show (see Section 3.3) a synthetic example illustrating the effect of additive noise on spectral ratio measurements and show that the impact of the ambient noise on our results is small.

Traces were also rejected from the analysis on the basis of low-quality shear-wave splitting analysis results and/or low signal-to-noise ratio. We were also careful to separate path-dependent effects from polarization and time-dependent effects. Therefore, only data from the source cluster nearest to the receivers were used (cluster 1 in Teanby *et al.* 2004). After selection of data using these restrictive criteria, only 35 pairs of seismograms remained. Only data from the top three geophones in the array were used for reasons of data quality.

3 RESULTS AND SENSITIVITY TESTING

3.1 Results

Typical seismograms (labelled event A and event B here), with estimates of noise spectra calculated from pre-signal noise, amplitude spectra, and $\log_e$ (amplitude spectral ratios) are shown in Fig. 2. In the data from event A, S1 has experienced more attenuation of high frequencies than S2. For event B the opposite is the case. No dependence of differential attenuation on downhole geophone number was observed. Pre-signal noise spectra were calculated using the same window lengths and tapers used in calculating the spectral ratios, and were chosen by hand to avoid any interfering events and to be representative of the noise level for that seismogram.

Note that the difference in peak amplitude between Event A and Event B is in the opposite sense to the amount of frequency-dependent attenuation experienced by each. This illustrates that the relative peak amplitudes of the split shear waves are more strongly dependent on the initial polarization of the incident shear wave than on relative levels of frequency-dependent attenuation.

Events A and B exhibit only small amounts of shear-wave splitting (splitting times are 2.5 and 3.0 ms respectively), yet their differential attenuation values are not among the smallest in magnitude. This need not be problematic as the only requirement for the shear wave to sense attenuation anisotropy is that it must have been split. It could potentially then pass through a region with high attenuation anisotropy but only very low-velocity anisotropy leading to a high differential attenuation but low splitting time.

Fig. 3(a) shows the temporal variation in minimum percentage anisotropy estimated from the shear-wave splitting analysis of Teanby *et al.* (2004). Fig. 3(b) shows the temporal variation in differential attenuation to allow comparison of temporal trends.

Correlation coefficients (R) were calculated for the 35 data points to test for relationships between differential attenuation and: minimum percentage anisotropy, fast direction, inclination, backazimuth, and the angle between the strike of the inferred initial source polarization and the inferred strike of the fast shear wave. These correlation coefficients and associated statistics are given in Table 1.

The inferred initial source polarization strike and the inferred strike of the fast shear wave are results obtained from the splitting analysis. They are the strikes of the planes containing the incident ray path and the best estimates of the initial source polarization and fast shear-wave polarization respectively. They were calculated as part of the splitting analysis of Teanby *et al.* (2004).

Given the small number of data points, leading to large uncertainties on R, the statistics in Table 1 are only a guide to potential correlations within the data. The results are consistent with there being correlations between differential attenuation and both the backazimuth and the angle between the strike of the inferred initial source polarization and the strike of the fast shear wave. The latter angle estimate is strongly dependent on the peak amplitude ratio between S1 and S2. A possible correlation may also exist between differential attenuation and minimum percentage anisotropy. Given the small variation in total traveltime for the events studied the minimum percentage anisotropy is strongly correlated with the splitting time, for this reason correlation results for splitting time are not shown. The inferred fast shear-wave strike, the inferred source polarization strike and the inclination are uncorrelated with the differential attenuation. Fig. 4 shows the data on which these correlation coefficients are based, since correlation coefficients presented on their own can be misleading.

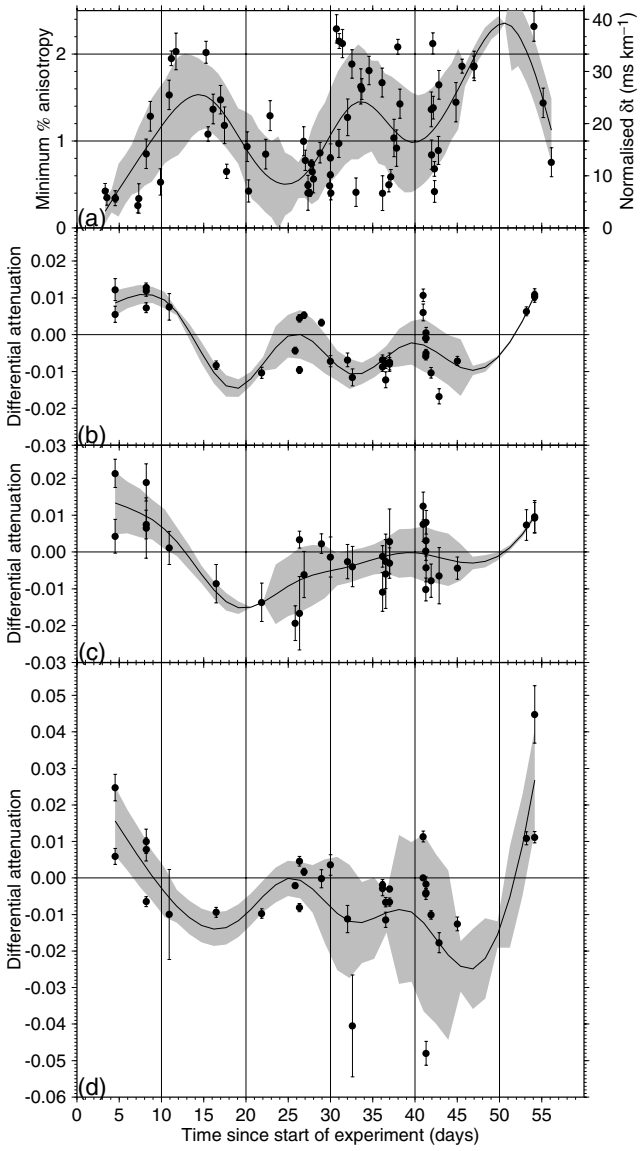

Figure 3. Comparison of (a) temporal variation of minimum percentage anisotropy derived from shear-wave splitting analysis (Teanby *et al.* 2004) with: (b) differential attenuation calculated using spectral ratios, a 2π multitaper, and a 222 ms long time window; (c) differential attenuation calculated using spectral ratios and a 101 ms long boxcar window and (d) differential attenuation calculated using matching filters, based on Raikes & White (1984). Best-fit curves and error envelopes are also plotted. Note the different ordinate scale on (d).

3.2 Sensitivity to parametrization

Our spectral-ratio-based analysis was repeated several times using different window lengths and taper types. In testing different taper types the data were not windowed with the peak amplitude in the same place relative to the window onset, as a sensible window position to use for each window type depends on the window shape. The temporal variation in differential attenuation was examined after analysis using window lengths of approximately 100, 150 and 200 ms (the data sampling interval is 1 ms), and boxcar, 50 per cent cosine, 100 per cent cosine tapers as well as a 2π Thomson adaptive multitaper (Thomson 1982). Some parameter testing was required before selection of the 2π multitaper. The general shape of the temporal variation in differential attenuation was robust to the taper type and window length used in the analysis. Of the tapers used, the multitaper appeared to give the least scattered results. As an example, Fig. 3(c) shows the differential attenuation as a function of time calculated using a 101 ms boxcar taper (i.e. no tapering). Note that this is an extreme case since of all the tapers tested this is the least appropriate for spectral ratio work due to its poor spectral leakage properties (e.g. Pujol & Smithson 1991).

It was not possible to produce meaningful tests of bandwidth sensitivity since the narrow signal bandwidth meant that after subdivision the signal bandwidth would be too small for useful attenuation estimates, and including data from outside the signal bandwidth would not be of interest in testing since it would obviously degrade the results. The bandwidth sensitivity may be tested with other microseismic data sets that are richer in frequency content.

3.3 Evaluation of the effects of additive noise on differential attenuation measurements

Additive noise within the signal bandwidth can cause serious problems for spectral ratio analyses. Alternative strategies to the formation of spectral ratios exist for estimating a transfer function in the presence of noise. One such strategy was proposed in the context of seismic Q estimation by Raikes & White (1984). Their method uses the geometric mean of two matching filters estimated in the frequency domain to transform one wavelet into the other, and vice versa. This allows the selection of a transfer function estimate that is not sensitive to the incoherent parts of the two traces (i.e. the parts that cannot be obtained by linear filtering of the other trace). The ordinary coherence, calculated during the process, gives an indication of a reliable bandwidth over which to perform the analysis, as does the region in which the two matching filter gains agree. The method also yields an estimate of the phase of the transfer function. For simplicity a 50 per cent cosine taper and a 222 ms window length were used within the matching filter method rather than the adaptive multitaper.

Fig. 3(d) shows the temporal variation in differential attenuation calculated using the matching filter method. Note that the ordinate scale has been changed to accommodate outliers. These correspond to points, which were estimated using only a very narrow signal bandwidth, as the coherence was low at all other frequencies. Apart from these outliers the results obtained using the matching filter method are similar to those obtained using spectral ratios, and show an approximately similar temporal variation. Although the matching filters have produced results that are consistent with the spectral ratio based results, they do not appear to have improved on the spectral ratio technique as one might have expected them to due to their capability for superior handling of the noise. We think that the reason for this lack of improvement may be that after the rotations involved in the splitting analysis, the noise on S1 and S2 is no longer statistically independent and so is not treated as noise in the matching filter method.

Ideally we would like to be able to subtract an estimate of the pre-signal noise from the amplitude spectra which are used to form the spectral ratios. Although our data are stationary enough to allow this, in practice such an approach is not workable for two reasons. First, the amplitude spectra of the signal and noise are not simply additive unless their phase spectra are the same. Second, the subtraction of the noise spectral estimates (which could be made more stable by estimating them over a longer time period and interpolating to the correct frequencies) can lead to holes in the spectrum, causing instability in the $\log_e$ (spectral ratios).

Table 1. Correlation coefficients (R) for differential attenuation, ΔQ^{-1}_{f-s}, tested against various experimental/splitting parameters. R is normalized to have a maximum value of one for a perfect correlation and a minimum of minus one for a perfect anticorrelation. P gives the probability of obtaining a correlation coefficient as large as $|R|$ in the absence of any true correlation. Also given are 95 per cent confidence limits on R. These provide a measure of the uncertainty in the correlation given the low number of data points. All results are given to 2 significant figures.

Variable correlation tested against ΔQ^{-1}_{f-s}	R	P	95 per cent confidence limits on R	Likelihood of correlation?
Backazimuth	0.64	0.000040	0.38–0.80	High
Angle between source polarization strike and fast direction strike	−0.60	0.00017	−0.77–−0.33	High
Minimum per cent anisotropy	−0.34	0.043	−0.61–0.012	Medium
Fast direction strike	0.20	0.25	−0.14–0.50	Low
Source polarization strike	0.19	0.28	−0.15–0.49	Low
Inclination	0.029	0.87	0.31–−0.36	Very low

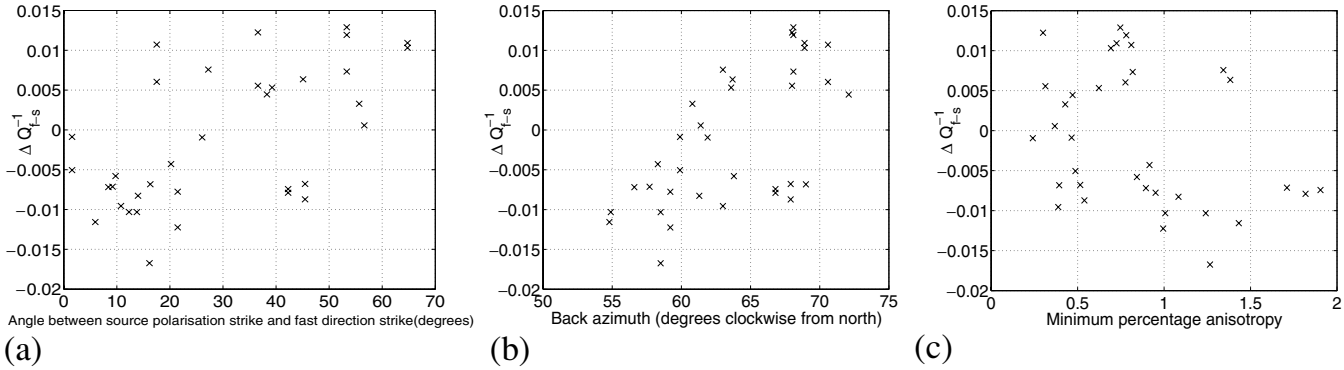

Figure 4. Differential attenuation plotted against: (a) the angle between the inferred source polarization strike and the inferred fast direction strike; (b) event backazimuth and (c) minimum percentage anisotropy. Error bars are not displayed to allow easier visual identification of trends. The approximate magnitude of the uncertainties on ΔQ^{-1}_{f-s} can be gauged from Fig. 3.

Fortunately the signal-to-noise ratio over the signal bandwidth is high for this data set. This can be seen from Figs 2(c) and (d), which shows that at the dominant frequency the noise is typically over 20 dB lower in amplitude than the weaker split shear wave.

3.4 Assessment of the impact of receiver response on differential attenuation measurements

The raw seismograms in our differential attenuation analysis have undergone several rotations. If the transfer function gains on the three components of a receiver differ, then any differential attenuation signature could be destroyed as there would be an artificial dependence of the measured differential attenuation due to the precise weightings of the original three components used to achieve a particular rotation. It was, therefore, necessary to examine the transfer functions of the three components of the receivers to test whether they were sufficiently similar in gain that the size of the differential attenuation studied was well above any false differential attenuation introduced by differences in the frequency-dependent gains of the three components.

During acquisition of the Valhall microseismic data set daily tests of the impulse responses of the six downhole three-component geophones were carried out. These 'ping tests' involved the application of a sharp step in voltage to each geophone component of each downhole geophone. The geophone outputs were recorded and the records used to assess the consistency of performance of the geophones. These records provide a means of assessing the frequency-dependent gain of the components and assessing whether or not the recording system is suitable for the analysis of differential attenuation of split shear waves.

For most of the days on which an event from our subset of data was recorded, the ping test recorded on the morning of that day was usable to assess the frequency-dependent gain of the components. On days where no ping test was available, a ping test from the previous day was used. Each ping test was rotated with the rotations used to process the real seismograms such that S1 and S2 were obtained on the two transverse components. Next the differential attenuation was calculated by regression of $\log_e$(spectral ratios) over the same bandwidth as was used in the analysis of the event. This procedure yielded a set of apparent differential attenuations that were due solely to differences in the transfer functions of the three components of each geophone. Fig. 5 shows the waveforms resulting from rotating an example ping test to simulate the geophone response to a pair of split shear waves, with corresponding amplitude spectra. Fig. 6 shows the resulting false differential attenuation obtained when the rotated ping tests were taken through the spectral ratio process. Note the dramatically different vertical scale compared to the results in Fig. 2(f). We assume here that the ping tests allow the estimation of the frequency-dependent responses of the geophone components and that geophone coupling is included in this response. Under this assumption the analysis shows that the differential attenuation observed cannot be coming from differences in the frequency-dependent gain or coupling of the geophone components.

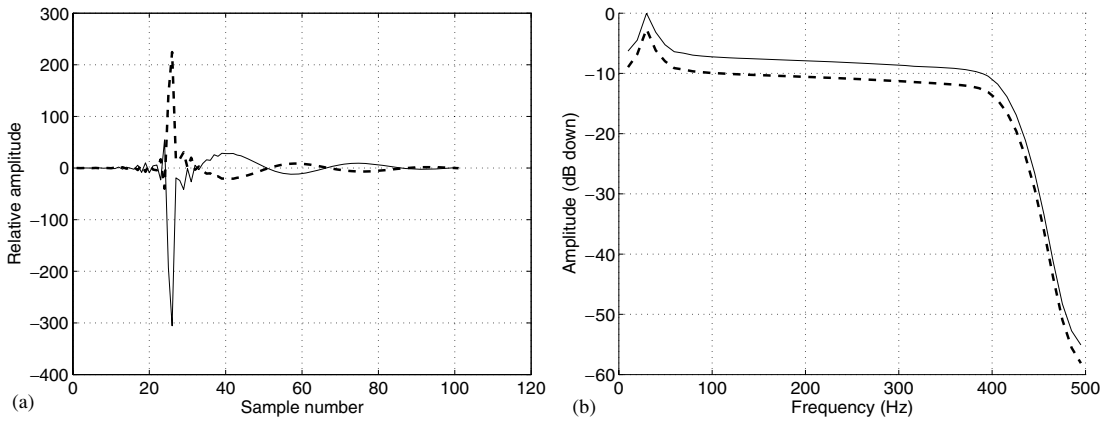

Figure 5. An example ping test, after rotation to simulate the splitting analysis performed on a shear-wave event from the same day.

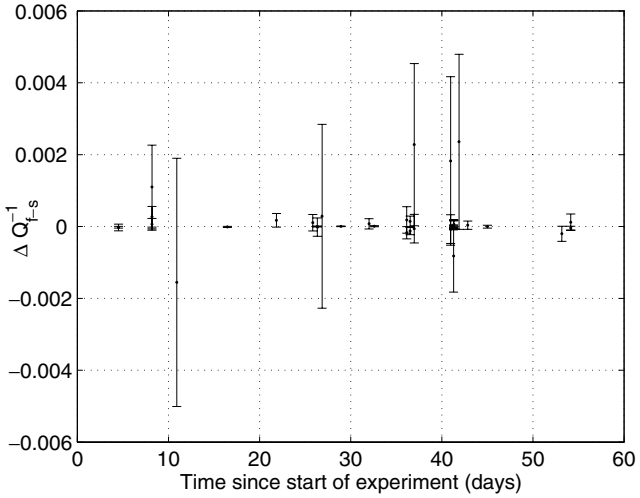

Figure 6. False attenuation values, plotted against time, resulting from different frequency-dependent gains on the three components of each downhole geophone.

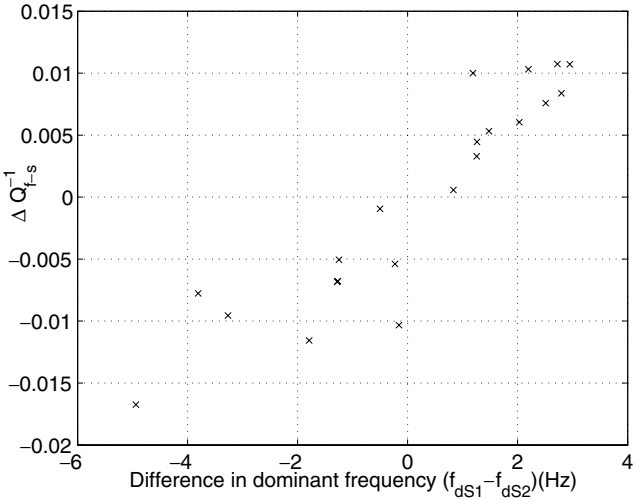

Figure 7. Difference in dominant frequency, $f_{dS1} - f_{dS2}$, plotted against differential attenuation.

3.5 Alternative methods of analysing relative frequency content

Centroid frequency shift methods (e.g. Quan & Harris 1997) can be more robust than spectral ratio methods for seismic attenuation estimation. In order to transform a centroid, or dominant frequency shift into an attenuation attribute however, it is necessary to choose a spectrum that is reasonably representative of the unattenuated spectrum in the field data. Unfortunately, the variation in spectral content between events in our data set was such that the choice of such a reference spectrum was problematic. For this reason centroid frequency shift methods were not used on these data. However, as a quality control measure we examined the difference in the dominant frequencies of S1 and S2 and compared it with the differential attenuation. Problems with our attenuation analysis would be highlighted if the dominant frequency did not shift in the expected sense given the sign of the differential attenuation.

The dominant frequency can be defined (Barnes 1993) as

$$f_d^2 = \frac{\int_0^\infty f^4 P(f)\, df}{\int_0^\infty f^2 P(f)\, df}, \tag{4}$$

where f_d is the dominant frequency, and $P(f)$ is the power spectrum. Fig. 7 shows the difference in dominant frequency between the two shear waves, $f_{dS1} - f_{dS2}$, calculated over the same bandwidth as the attenuation attribute against which it is plotted. The correlation coefficient, $R = 0.9163$, with a P value (see Table 1) of 5.47×10^{-9} and a 95 per cent confidence interval from 0.8018–0.9659. The dominant frequency shift is, therefore, very well positively correlated with the differential attenuation showing that the dominant frequency is shifting in the correct sense. This implies that the differential attenuation effect is real and not an artefact of the method used to measure it.

4 DISCUSSION AND CONCLUSIONS

We have presented a simple new methodology for analysing the frequency content of split shear waves, which could easily be applied in the future to other data sets, some of which may have a broader signal bandwidth and so be more suitable for such an analysis.

The differential attenuation shows a temporal variation. The locations of the peaks and troughs in time approximately mirror those in the minimum percentage anisotropy changes with time reported by Teanby *et al.* (2004).

An interesting result presented in this paper is the observation that sometimes S1, the fast shear wave, can be poorer in high frequencies than S2, the slow shear wave. This observation is robust to the parametrization of the method used to calculate the differential attenuation. This observation is contrary to the attenuation anisotropy predicted by the effective medium model of Hudson (1981) for the elastic moduli likely to be encountered in our experiment.

The differential attenuation appears to correlate with both the backazimuth and with the angle between the initial source polarization strike and the strike of the fast shear wave polarization (both derived from the splitting analysis). Since this angle and the backazimuth are also correlated a single mechanism could be responsible for both of these correlations.

The correlation between the differential attenuation and the angle between the initial source polarization strike and the strike of the fast shear wave polarization means that there is also a correlation between the differential attenuation and the peak absolute amplitude ratio, since the main controlling influence over this amplitude ratio should be the angle between the initial polarization and the fracture plane, which controls in what proportions the initial shear wave is split. A contribution is made to the correlation between the peak absolute amplitude ratio and differential attenuation by the effect of variation in signal-to-noise ratios within the numerator and denominator of the spectral ratios. This is difficult to correct for, and we are investigating the best method of eradicating this effect.

Our method is based on the linear regression of LASRs, however many of the LASRs obtained were non-linear over the signal bandwidth. This led to a reduction in the number of time-series available for analysis. The non-linearity could be caused by noise contamination, unlikely given the high signal-to-noise ratio of the data, or perhaps by preferential scattering of some frequencies. Alternatively the attenuation mechanisms operating on one or both of the split shear waves may not be a constant-Q mechanism. This effect was not examined in detail, since the limited signal bandwidth, typically about 20–80 Hz (for the ≈200 ms long data segments) meant that any conclusions reached about the frequency dependence of the differential attenuation would be highly inaccurate and measured over only a small bandwidth. Microseismic data sets with larger bandwidth do, however, exist, and it would be interesting to examine the gain and phase of the transfer function between S1 and S2 on such a data set.

If present, local structures in the subsurface close to the receiver array could lead to differential amplification on the components, potentially causing significant distortion of the results. However, previous work on source location at Valhall (DeMeersman 2005) contains no evidence for such problematic structures near the receiver array.

The behaviour of the dominant frequency estimates tends to support the robustness of our differential attenuation observations, as does the high signal-to-noise ratio within the signal bandwidth, and the small effect of the differences in frequency-dependent gain on the three components of the geophones used.

In this analysis we are assuming that the initial frequency content of the split shear waves is identical. We also assume that the method used for the splitting analysis, which does not take attenuation explicitly into account, is robust enough that the distortion of the waveforms by attenuation does not cause serious errors in the results. We intend to investigate this in future experiments.

Only those events with high-quality splitting results and linear $\log_e$ spectral ratios were included in our analysis. For approximately half of these events the faster split shear wave is poorer in high frequencies than the slower split shear wave. The mechanism causing this effect is currently unclear. As a result of considerable sensitivity testing we feel that both this observation and the temporal variation in differential attenuation are robust to variations in the parametrization of the method used to obtain it.

ACKNOWLEDGMENTS

This work was supported by ABB Offshore Systems, BP Norge, Schlumberger Cambridge Research, and Shell Exploration and Production UK. ABB and BP provided microseismic data. The views in this paper are those of the authors and not necessarily those of the organizations, which supported the work. We thank Mark Chapman and Martha Savage for reviews that have improved this paper. We thank Rob Jones and Mirko van der Baan for useful discussions.

REFERENCES

Aki, K. & Richards, P.G., 1980. *Quantitative Seismology—Theory and Methods*, W.H. Freeman, San Francisco.

Backus, G.E., 1962. Long-wave elastic anisotropy produced by horizontal layering, *J. geophys. Res.,* **67,** 4427–4440.

Båth, M., 1974. *Spectral Analysis in Geophysics*, Elsevier, Amsterdam.

Barnes, A.E., 1993. Instantaneous spectral bandwidth and dominant frequency with applications to real seismic reflection data, *Geophysics,* **58,** 419–428.

Caley, A.J., Kendall, J.-M., Jones, R.H., Barkved, O.I. & Folstad, P.G., 2001. Monitoring fractures in 4D using microseismic data, *Extended Abstracts, EAGE 63rd Conference and Technical Exhibition,* **1,** F–23.

Chapman, M., 2003. Frequency-dependent anisotropy due to meso-scale fractures in the presence of equant porosity, *Geophys. Prospect.,* **51,** 369–379.

Chapman, M., Zatsepin, S.V. & Crampin, S., 2002. Derivation of a microstructural poroelastic model, *Geophys. J. Int.,* **151,** 427–451.

Chesnokov, E.M., Queen, J.H., Vichorev, A., Lynn, H.B., Hooper, J., Bayuk, I., Castagna, J. & Roy, B., 2001. Frequency-dependent anisotropy, *Expanded Abstracts, 71st Ann. Int. SEG Mtng.,* 125.

Crampin, S. & Chastin, S., 2003. A review of shear wave splitting in the crack-critical crust, *Geophys. J. Int.,* **155,** 221–240.

Crampin, S. & Zatsepin, S.V., 1997. Modelling the compliance of crustal rock—II. response to temporal changes before earthquakes, *Geophys. J. Int.,* **129,** 495–506.

De Meersman, K., 2005. Estimating signal polarisations in seismic array data: theory and applications, *PhD thesis*, 143pp., University of Leeds, UK.

Dyer, B.C., Jones, R.H., Cowles, J.F. & Barkved, O., 1999. Microseismic monitoring of a North Sea Reservoir, *World Oil,* **220**(3), 74–78.

Futterman, W.I., 1962. Dispersive body waves, *J. geophys. Res.,* **67,** 5279–5291.

Gardner, G.H.F., Gardner, L.W. & Gregory, A.R., 1974. Formation velocity and density—the diagnostic basics for stratigraphic traps, *Geophysics,* **39,** 770–780.

Hudson, J.A., 1981. Wave speeds and attenuation of elastic-waves in material containing cracks, *Geophys. J. R. astr. Soc.,* **64,** 133–150.

Liu, E., Queen, J.H., Li, X.-Y., Chapman, M., Lynn, H.B. & Chesnokov, E.M., 2002. Analysis of fracture-dependent seismic anisotropy from a multicomponent VSP, *Expanded Abstracts, 72nd Ann. Int. SEG Mtng.,* 101–104.

Marson-Pidgeon, K. & Savage, M.K., 1997. Frequency-dependent anisotropy in Wellington, New Zealand, *Geophys. Res. Lett.,* **24**(24), 3297–3300.

Maultzsch, S., Chapman, M., Liu, E. & Li, X.Y., 2003. Modelling frequency dependent seismic anisotropy in fluid-saturated rock with aligned fractures: implications of fracture size estimation from anisotropic measurements, *Geophys. Prospect.,* **51,** 381–392.

Peacock, S., McCann, C., Sothcott, J. & Astin, R.T., 1994. Seismic velocities in fractured rocks: an experimental verification of Hudson's theory, *Geophys. Prospect.,* **42,** 27–80.

Pointer, T., Liu, E. & Hudson, J.A., 2000. Seismic wave propagation in cracked porous media, *Geophys. J. Int.,* **142,** 199–231.

Pujol, J. & Smithson, S., 1991. Seismic wave attenuation in volcanic rocks from VSP experiments, *Geophysics,* **56,** 1441–1455.

Quan, Y. & Harris, J.M., 1997. Seismic attenuation tomography using the frequency shift method, *Geophysics,* **62,** 895–905.

Raikes, S.A. & White, R.E., 1984. Measurements of earth attenuation from downhole and surface seismic recordings, *Geophys. Prospect.,* **32,** 892–919.

Rathore, J.S., Fjaer, E., Holt, R.M. & Renlie, L., 1995. Acoustic anisotropy of a synthetic sandstone with controlled crack geometry, *Geophys. Prospect.,* **43,** 805–829.

Spencer, T.W., 1985. Measurement and interpretation of seismic attenuation, in *Developments in Geophysical Exploration Methods*, Vol. 6, pp. 71–109, ed. Fitch A. A., Elsevier Applied Science, Barking, UK.

Teanby, N., Kendall, J.-M., Jones, R.H. & Barkved, O., 2004. Stress-induced temporal variations in seismic anisotropy observed in microseismic data, *Geophys. J. Int.,* **156,** 459–466.

Thomsen, L., 1995. Elastic anisotropy due to aligned cracks in porous rock, *Geophys. Prospect.,* **43,** 805–829.

Thomson, D.J., 1982. Spectrum estimation and harmonic analysis, *Proc. IEEE,* **70,** 1055–1096.

Tod, S.R. & Liu, E., 2002. Frequency-dependent anisotropy due to fluid flow in bed-limited cracks, *Geophys. Res. Lett.,* **29,** doi:10.1029/2002GL015369.

Werner, U. & Shapiro, S.A., 1999. Frequency-dependent shear-wave splitting in thinly layered media with intrinsic anisotropy, *Geophysics,* **64,** 604–608.

Zatsepin, S.V. & Crampin, S., 1997. Modeling the compliance of crustal rock: I—response of shear-wave splitting to differential stress, *Geophys. J. Int.,* **129,** 477–494.

APPENDIX A: DIFFERENTIAL ATTENUATION AND VELOCITY ANISOTROPY PREDICTED AT VALHALL BY THE THEORY OF HUDSON (1981)

Hudson (1981)'s effective medium theory predicts the velocity and attenuation anisotropy due to a dilute concentration of aligned penny-shaped cracks. It predicts how the attenuation varies as a function of the angle between the direction of propagation and the crack normal. This appendix is intended to give an indication of the velocity and attenuation anisotropy predicted for our microseismic experiment at Valhall using this theory, to allow easy comparison with our observations.

In what follows, the version of Hudson (1981)'s theory dealing with fluid-filled cracks is used with a crack aspect ratio of 0.0001 and the parameters given in Table A1.

This effective medium theory is described in terms of the vertically polarized split shear wave (*SV*), and the horizontally polarized split shear wave(SH). The ratio of the *SH* wave speed to the *SV* wave speed is sensitive to the crack density and the angle between the direction of travel and the crack normal. Fig. A1 shows the wave speed ratio over a range of angles for the parameters given in Table A1 and a range of crack densities. Note that *SH* becomes faster than *SV* at angles larger than 60 degrees to the crack normal. In other words, for angles of incidence less than 60 degrees *SV* is S1, for angles greater than 60 degrees *SH* is S1. Note that this crossover effect is not predicted for gas-filled fractures.

Table A1. Parameters used in effective medium models for Valhall microseismic data. α and β are respectively the *P*-wave and shear-wave speeds in the uncracked solid; ρ is the density of the uncracked solid, estimated from α using Gardner's equation (Gardner 1974); and κ' is the bulk modulus of the fluid filling the cracks.

α (ms^{-1})	β (ms^{-1})	ρ (kg m^{-3})	κ' (N m^{-2})
1350	590	1879	2.25×10^9

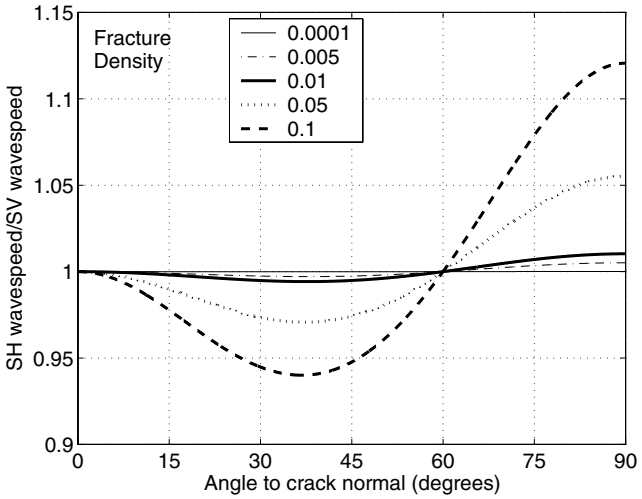

Figure A1. The ratio of *SH* wave speed to *SV* wave speed for a range of fluid-filled crack densities, an aspect ratio of 0.0001, and the parameters in Table A1.

The ratio of *SH* attenuation (i.e. Q^{-1}) to *SV* attenuation is only very slightly sensitive to the crack aspect ratio. Fig. A2 shows the variation of the ratio of *SV* attenuation to *SH* attenuation. Only the curve for an aspect ratio of 0.0001 is shown, since all curves from aspect ratios of 0.0001–0.1 are indistinguishable plotted at this scale. Beyond 60 degrees to the crack normal the ratio continues to increase rapidly to an extremely high value at 90 degrees. At angles less than 60 degrees to the crack normal the *SH* wave (S2) is preferentially attenuated, beyond 60 degrees the *SV* wave (again S2) is preferentially attenuated. This model, therefore, predicts, for the situation of our microseismic experiment at Valhall, that the faster split shear wave should always be the least attenuated.

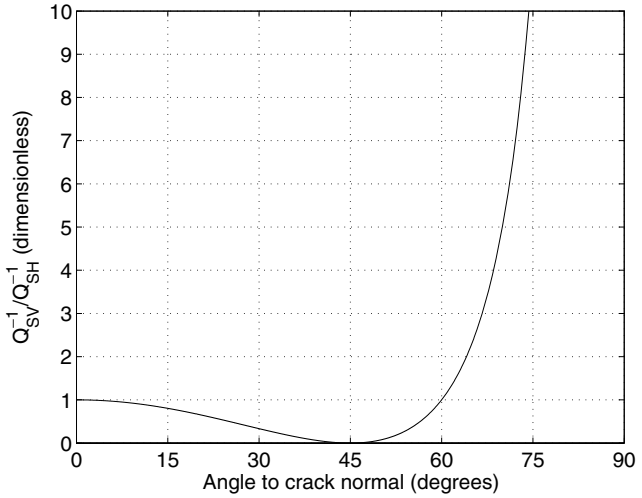

Figure A2. The ratio of *SV* attenuation to *SH* attenuation for an aspect ratio of 0.0001 and the parameters in Table A1.